

Accepted by MNRAS, 10th July 2000

The Optical Velocity of the Antlia Dwarf Galaxy¹

Eline Tolstoy^{2 3}

European Southern Observatory, Karl-Schwarzschild-str 2, D-85748, Garching bei München, Germany

Michael Irwin⁴

Institute of Astronomy, University of Cambridge, Madingley Road, Cambridge, CB3 0HA, England, UK

ABSTRACT

We present the results of a VLT observing program carried out in service mode using FORS1 on ANTU in Long Slit mode to determine the optical velocities of nearby low surface brightness galaxies. Outlying Local Group galaxies are of paramount importance in placing constraints the dynamics and thus on both the age and the total mass of the Local Group. Optical velocities are also necessary to determine if the observations of HI gas in and around these systems are the result of gas associated with these galaxies or a chance superposition with high velocity HI clouds or the Magellanic Stream. The data were of sufficient signal-to-noise to obtain a reliable result in one of the galaxies we observed - Antlia - for which we have found an optical helio-centric radial velocity of 351 ± 15 km/s.

Subject headings: GALAXIES: INDIVIDUAL: ANTLIA, GALAXIES: KINEMATICS AND DYNAMICS, GALAXIES: LOCAL GROUP

¹Based on observations collected at the European Southern Observatory, Chile, in service mode, proposal number 63.N-0197

²Current address: UK GEMINI Support Group, University of Oxford, Nuclear and Astrophysics Laboratory, Keble Road, Oxford OX1 3RH, UK

³email: etolstoy@astro.ox.ac.uk

⁴email: mike@ast.cam.ac.uk

1. Introduction

Several relatively isolated outlying members of the Local Group: Tucana, Phoenix, Cetus and Antlia currently have no measured optical radial velocities. Although Phoenix (Carignan *et al.* 1991; St-Germain *et al.* 1999), Antlia (Fouqué *et al.* 1990) and possibly Tucana (Oosterloo *et al.* 1996), have tentative HI detections, there are as yet no compelling reasons to believe that any of the detected HI is necessarily associated with the optical galaxy (*e.g.* Young & Lo 1997). These outlying members of the Local Group are of paramount importance in determining membership and dynamics of the Local Group and in particular for placing tight constraints on both the age and total mass of the Local Group. In the case of Phoenix an optical radial velocity is needed to assess possible membership as the outermost satellite system of our Galaxy; thereby constraining the mass of the Galactic Halo out to the unprecedented distance of 400 kpc.

Optical radial velocities can be used to directly probe the relationship between HI gas detections in and around dwarf spheroidal galaxies (dSphs), coincident line-of-sight Galactic high velocity clouds (*e.g.* Braun & Burton 2000), or high velocity clouds associated with the Magellanic Stream. This is one of a number of open questions in the attempt to establish if a link exists between dSphs with no gas in their centres and gas rich, currently star-forming, dwarf irregular galaxies. Proving that gas is associated with dSphs would give support to the idea that HI gas can be severely disrupted, perhaps during a star formation episode, blown into an extended dark matter halo, but still retained (*e.g.* Sculptor, Carignan *et al.* 1998).

However, obtaining accurate radial velocities of these faint and diffuse objects has required the availability of Southern 8m-class telescopes. In this paper we present the results of VLT/FORS1 long slit observations of three of the isolated, outlying members of the Local Group: Antlia, Cetus and Tucana (see Table 1). All of these galaxies are close enough such that their stellar populations are easily resolved, and none have previously measured optical velocities. Unfortunately, due to weather conditions and the proximity of the Moon for two sets of observations, only the data for, Antlia, was of sufficient signal-to-noise to give a reliable result, but for completeness we have included an outline description of the other data.

Antlia has been discovered more than once; in the radio, via an HI survey by Fouqué *et al.* (1990) and in the optical, where it was first confirmed as a member of the Local Group by Whiting *et al.* (1997). Antlia is a companion galaxy (on the sky) to NGC 3109, which is within the measurement errors at the same distance, and has a comparable HI radial velocity ($v_{\odot}(\text{HI}) = 361 \text{ km/s}$ compared to 403 km/s for NGC 3109). However, the HI gas

has also been suggested to be a chance superposition with a side-lobe of the HI detected in NGC 3109 (*e.g.* Blitz & Robishaw 2000). More recent VLA data however suggests that the HI is in fact associated with Antlia (Skillman, private communication). Measuring an optical velocity for Antlia would not only clarify the whole situation but also add weight to the hypothesis that most, if not all, dSphs have associated HI gas.

Tucana, which is also a relatively recently discovered member of the Local Group (Lavery & Mighell 1992), lies close to the line-of-sight of the Magellanic Stream and as such it is hard to assess the significance of the discovery of nearby HI gas by Oosterloo *et al.* (1996). Tucana is at a distance of 900 kpc, and lies on the opposite side of the Local Group to the M31 sub-system. Until the discovery of Cetus, it was the only known unambiguously isolated dSph in the Local Group, and therefore a unique probe of the galactic evolution and internal dynamics of an isolated dSph.

Cetus is a newly discovered galaxy in the Local Group (Whiting *et al.* 1999) about which very little is known. Although located in the general direction of the extension of the Local Group toward the Sculptor group, Cetus appears to be an isolated dSph and as such may join the class currently occupied only by Tucana. The first deep CMD of Cetus, which reaches down to the level of the horizontal branch (HB) shows this to be predominantly old system with a highly populated HB and no signs of recent (<1Gyr old) star formation (Tolstoy *et al.* 2000). Preliminary attempts to detect Cetus in the HIPASS survey (see Whiting *et al.* 1999) have revealed nothing, which suggests that Cetus does not contain any HI gas. Therefore, the only way to learn more about its position in the Local Group, and if it really is an isolated system, is to measure an optical radial velocity.

2. Observations

The observations were obtained in service-mode, with UT1/FORS1 in the Long Slit Spectroscopy (LSS) instrument set-up, between May and August 1999 (see Table 2). The FORS1 long slit spans 6.8 arcmin and was used with a slit width of 1 arcsec and the GRIS-600I+15 grism along with the OG590 order-sorting filter, to cover the Ca II triplet wavelength region with as high resolution as possible. With this setting the pixel sampling is close to 1Å per pixel and the resolution \approx 2-3Å over the wavelength range 7050–9150Å. This is the maximum resolution that can be obtained with FORS1 without resorting to a narrower slit. Although this is a wavelength range at which the FORS1 CCD (Tektronix) has reduced sensitivity it is where the red giant stars we were aiming to detect are brightest. The Ca II triplet is also a useful unblended feature to accurately measure radial velocities

(*e.g.* Hargreaves *et al.* 1994) and there are abundant narrow sky lines in this region for wavelength calibration and/or spectrograph flexure monitoring.

Our observation request consisted of two different slit positions per target galaxy, or in ESO parlance two separate Observation Blocks (OBs), which could be (and indeed were) observed on different nights, and in different conditions (see Table 2). Although we did not have very strict observing constraints (seeing $< 1\text{arcsec}$, any weather), most of our data were taken out of specifications, either because the seeing was worse, or the moon constraint was violated. Two of the three galaxies (Cetus and Tucana) in our sample were taken in full moon (96% and 100% illumination) conditions and Cetus was only 30 degrees away from the moon. These poorer than anticipated conditions with no corresponding increase in exposure time, combined with the reduction in the sensitivity of the system from the initial values obtained with the exposure time calculator, meant all the data ended up of much lower signal-to-noise than anticipated.

Each OB was made up of a target observation in conjunction with a sequence of radial velocity (rv) standards (both individual K-giants and bright globular clusters, see Table 3). The K-giant absolute rv standards provided the basic velocity standardization in addition to Ca II triplet template spectra for comparison with the much lower signal-to-noise dwarf galaxy spectra. By observing bright globular clusters with known radial velocities we further sought to test our methodology with data more closely resembling the primary targets. A useful by-product of this is additional template spectra to cross-correlate with the main target objects.

Typically we observed at two different slit positions on each target galaxy, and sometimes also on the calibration globular clusters. We attempted to align the slit to cover known, likely, stellar members where possible, but for some systems we lacked suitable pre-imaging exposures with a world coordinate system to use as input into the FIMS, the tool used to make OBs for execution at the telescope. In the latter case it was a reasonable assumption that we would hit several objects per slit as these galaxies are fairly densely populated by (faint) stars. We also planned to use the combined integrated unresolved light of the underlying galaxy across the slit.

In the case of Antlia and Rup 106 one of our OBs was executed twice (no explanation given), with the result that instead of two separate target slit positions we had one. This had the (unanticipated, but interesting) benefit that we could check the repeatability of our results as these two OBs were observed one month apart.

3. Data Reduction and Calibration

All basic calibration data provided for UT1+FORS1 observations, *i.e.* not only bias frames, but also flat-field frames and arcs for wavelength calibration, are obtained during daylight hours. Because our observations require us to make very accurate determinations of the wavelength solution and because we are typically looking at very faint objects we were very careful in assessing the usefulness of the (day-time) calibrations provided and the potential for spectrograph flexure between arc calibration measurements and target measurements on sky. We were seriously concerned about the possibility of flexure of this Cassegrain-mounted spectrograph, between the daytime wavelength calibrations and the nightly observations, and also the long term effects since our data were taken over a period of a few months, which could easily introduce systematic wavelength offsets between data sets.

The default lamp flat fields provided included a multitude of spurious artifacts at a variety of scale-lengths rendering them difficult to use for sensitivity corrections. Similar spurious internal reflections also made the arc calibrations frames difficult to use, since in long-slit mode it is essential to accurately trace the spatial curvature of the spectral lines and extract an accurate two-dimensional wavelength solution. We also had several basic problems with the calibration data for the first OB (Antlia, taken in May 1999) because all the provided bias, flat-field and arc calibration frames were taken using four-quadrant readout mode, whereas the nightly observations used single-channel readout.

Because of these problems we made an executive decision to not use any of the daytime calibrations to either flat-field or wavelength calibrate the data. Most of the difficulties with the daytime calibration seem to stem from the reflections caused by the calibration lamps which live within FORS1 and are shone out of the instrument through the LADC (linear atmospheric dispersion corrector, *i.e.* two large pieces of glass) and bounced off the (closed) beam shutter back through the LADC before making it to the spectrograph slit. Not surprisingly there are reflections due to scattered light in the resulting calibration data.

The problems with the provided calibration data forced us to adopt a more creative approach than normal using the following steps all of which were done using the IRAF package.¹

Fortunately the fixed pattern bias is quite stable and there were sufficient single

¹IRAF is distributed by the National Optical Astronomy Observatories, which are operated by the Association of Universities for Research in Astronomy, Inc., under cooperative agreement with the National Science Foundation.

readout bias frames for this CCD taken over this period in the ESO archive. These were used to construct a master bias frame which, together with the under/overscan regions within the spectroscopic data, was used to trim and bias-correct all the data.

In the ESO archive there were also I broad-band filter twilight flat-field frames available taken using the same CCD. Since this covers the same wavelength region as the spectroscopic observations, we were able to use these to produce a high quality flat-field frame which could be used on the spectroscopic images. Illumination gradients across the flat were mapped using a combination of median and Gaussian filtering to produce a smooth two-dimensional illumination map. The stacked flat-field frame was then divided by the smooth illumination map and the result used to correct all the spectroscopic data for the pixel-to-pixel sensitivity variations/defects of the CCD in the standard manner.

Working in the wavelength range 7050–9150Å, at a resolution of 1Å/pixel, the night sky lines are plentiful and well distributed over the wavelength range and could be used to directly map the two-dimensional wavelength distortion and accurately calibrate the spectra. The adopted reference wavelengths were taken from the on-line Keck LRIS skyline plots, which were in turn based on a compilation by Osterbrock & Martel (1992). The two-dimensional distortion corrections were found to be stable to $\approx 0.1\text{Å}$ within an observing night, apart from small global translations (flexure) along the dispersion axis, and could therefore be used for the generic two-dimensional wavelength calibration of all the data for that night. This could otherwise have been a serious problem since the radial velocity standards do not have any significant skylines visible due to their much shorter exposure times. Additional checks and corrections for systematic wavelength shifts were made using the final extracted spectra and are described later.

We stress again that since it was not allowed telescope practice to take calibration arcs before and after each integration to monitor the instrument flexure (advertised to be zero at any distance from the zenith), we used the sky lines in the final extracted spectra to both measure and correct for this flexure. The variation in apparent sky line wavelengths indicated that although the flexure is small, and certainly never much bigger than a pixel, or ~ 35 km/s, it is not negligible, and not surprisingly, it is strongly dependent on zenith distance (see Table 4).

Each target observation of a dwarf spheroidal galaxy consisted of $3 \times 1800\text{s}$ exposures. There were no measurable internal shifts found for frames within a sequence, so these were combined in a straight-forward manner eliminating cosmic ray events, prior to wavelength calibration, carried out using the night sky lines. Globular cluster observations were typically integrations of 150–250s which were treated in the same way as the target galaxy observations.

The position of the slit across the central region of Antlia taken from the FIMS file used to prepare the OBs is shown in Figure 1. Also marked are four of the stars clearly detected in the Antlia spectra. The position of all the resolved objects detected in the Antlia long-slit spectra are plotted on the Colour-Magnitude Diagram (CMD) of Antlia (from Tolstoy 1999) in Figure 2. From the location on the CMD, and also position on the slit, stars B, C and D are all very likely to be members of Antlia, while A and E are much too bright to be associated with Antlia. Object F appears to be a background galaxy in the slit. The identification of all the resolved objects in the slit and their location on the CMD provides an excellent independent corroboration of the optical velocity determinations and was actually computed after the results from the spectroscopy were known.

4. Extracting and Wavelength Calibrating the Spectra

For the globular clusters and dSphs, image sections summed along the spatial axis were used to identify resolved stellar, or background galaxy images, in the slit and also to define the underlying unresolved background of the dwarf spheroidal galaxy for spectroscopic extraction. Spectra for these objects plus the integrated background were then extracted in the usual manner taking care to optimise the region chosen to represent the local sky. The computed sky spectrum was also extracted contemporaneously for later use in checking the wavelength solution systematics (see Figure 3). For the radial velocity standards contributions to systematics from slit centering of the extremely bright stars is also an issue that limits the achieved final accuracy and is reflected in the scatter ($\sigma_v \sim 5\text{km/s}$) of the derived velocities for the standards in Table 4.

In more detail:- The IRAF task IDENTIFY was used to make the wavelength calibration using the Keck LRIS sky-line identifications. The reference image used for this was always one of the coadded $3 \times 1800\text{s}$ dSph summed frames on a nightly basis. Next the task REIDENTIFY was used to trace the sky lines to track the two-dimensional distortion. FITCOORDS is then used to produce a two-dimensional polynomial distortion transformation which was input to TRANSFORM, *i.e.* to straighten out, the long-slit distortions. In all cases a single distortion mapping was stable enough to be used within a given nights observations. At this point the IRAF task APALL was used to extract both object spectra and sky spectra in the neighbourhood of each object in the usual manner.

The extracted one-dimensional sky spectra were then cross-correlated, using task FXCOR, against the reference image sky spectra, after continuum removal and suitable apodizing, to measure the stability of the wavelength solution and hence determine

the flexure of the spectrograph. The cross-correlation of sky lines within a single two-dimensional frame gives negligible velocity shifts of ± 3 km/s which is comparable to the juxtaposition of the wavelength calibration errors and correlation-function estimation errors.

Monitoring the wavelength stability of the radial velocity standards was more challenging. The globular clusters Rup 106, NGC 6752 and Pal 12, provided a link between the deeper sky exposures of the target dSphs and the radial velocity standards where no sky emission lines are visible. First the globular cluster extracted object sky spectra were cross-correlated with the dSph reference spectra to place them on the same zero-point system with an accuracy of ≈ 3 km/s. Then using a Gaussian fit to the lower half of the atmospheric A-band sky absorption features in the globular cluster spectra and the radial velocity standards spectra, the wavelength system of the radial velocity standards could be tied to the globular cluster spectra. The error in the location of the A-band was found to be ≈ 5 km/s using this fitting procedure, when there was good signal-to-noise. After adopting this bootstrapping of the wavelength solution, a series of internal consistency checks indicated the overall final systematics of the wavelength solution are in the range 5-10 km/s, more than adequate for the current goal.

The largest flexures found amounted to about 1 pixel and were found between the two Antlia data sets taken on different nights one month apart and for one of the radial velocity standards taken at an airmass of 2.4 on the same night as the primary wavelength calibration data (see Table 4).

5. Determining the Radial Velocities

In the previous section we described how we have extracted spectra and carried out a number of tests to determine the errors due to the wavelength calibration and correct for them. Now we can make an accurate comparison of the velocities of the lines in the Ca II triplet in all our observations and be confident that any offsets between the radial velocity standards, the cluster observations and dSphs are all representations of the true velocity differences (limited by signal-to-noise) between these objects and thus allow us to estimate the true optical velocity of the target galaxies.

One of the radial velocity standards, HD 107328 of spectral type K1 III, was used as the primary cross-correlation template. First, an order 12 cubic spline continuum fit was made and subtracted from the template spectrum. Then the IRAF SPLOT package

was used to snip out featureless regions from the continuum-subtracted template and to also remove the sky A-band absorption feature at $\approx 7600\text{\AA}$ by setting these regions to zero. This gives unit weight to those spectral regions with maximal information for radial velocity determination (*i.e.* unambiguous stellar absorption features) and zero weight to all other regions. Even the regions between the Ca II triplet lines were set to zero to minimise problems with residual sky line features causing zero velocity cross-correlation locking.

Radial velocities were then measured for all the spectra, using the standard Fourier cross-correlation package in IRAF, FXCOR. An example of the results for Antlia is shown in Figure 4. The measured radial velocity was then corrected for: the template radial velocity offset; the topo-centric correction to a helio-centric system; and for flexure. All of the measurements, the corrections and the final values for the individual objects extracted from the spectra are listed in Table 4, including Antlia, the radial velocity standards and the globular clusters Rup 106 and NGC 6752. The results for Pal 12, Cetus and Tucana were of such poor quality that no useful information on their radial velocities could be obtained at all.

For all the globular cluster and dSph observations, individual resolved objects were extracted separately in an attempt to identify system members and possible foreground star, or even background galaxy, interlopers. In addition to the individual objects in Antlia we also extracted the majority of the unresolved flux, plus central objects, in an attempt to boost the signal-to-noise. Three of the extracted spectra for Antlia (b,c,d) had radial velocities that matched within the errors and were also found later to lie at the tip of the red giant branch (see CMD in Figure 2). The summed spectra for Antlia stars B, C, D in the Ca II triplet region is shown in Figure 3, together with the vertically offset spectrum for NGC 6752 and an example sky spectrum. The Ca II triplet features in Antlia are clearly visible, redshifted by about 10\AA from those of NGC 6752. Note also how the strong night sky lines, plotted scaled down by a factor of 75 with respect to the Antlia spectrum, cause residual sky features even in the summed Antlia spectrum, emphasizing the crucial importance of careful template construction to avoid sky line residual locking. The final result for Antlia is an optical helio-centric radial velocity of 351 ± 15 km/s. The error estimate includes a contribution from the *rms* FXCOR estimation errors and the systematics of the whole wavelength calibration procedure, which contribute in roughly equal measure.

The same analysis was carried out identically for Tucana and Cetus. In both these cases the extremely bright sky lines and poor signal-to-noise due to full moon make the extracted spectra too poor to be of any use.

6. Conclusions

It is clear from the results of the individual stars observed in Antlia (and also in Rup 106 and NGC 6752) when we pick up a star which is member of the system and when we find a foreground, or in the case of Antlia-1-F a background galaxy. The previously acquired VLT Antlia images were used to select two candidate stars to lie on the slit (B,C), whilst (A, D, E) serendipitously turned up in the slit. The three stars B, C, and D are consistent with membership of Antlia both on account of their position in a Colour-Magnitude Diagram and their consistent optical velocities which are not likely to be similar to any objects of similar colour and magnitude in our galaxy.

In more detail, if the stars B, C and D in Antlia were Galactic and in the disk they would have a radial velocity with respect to the LSR of ~ 360 km/s and if they are Halo objects the galactocentric radial velocity is more appropriate at ~ 150 km/s. Contamination by disk K-dwarfs seems highly unlikely on two counts: the extremely high LSR-corrected radial velocity; and the distance any putative K-dwarfs would have to be. At $V \sim 23$ a typical K-dwarf would have a distance modulus of ~ 15 and would have to be at around 10 kpc distance and hence ~ 4 kpc above the Galactic Plane. In the case of possible Halo star K-giant contamination; the radial velocity is high but still around the 2σ Halo velocity dispersion. However, we can rule out K-giants due to distance constraints, since a typical K-giant at $V \sim 23$ would have a distance modulus over 25 and hence be at a distance of order 1 Mpc or more. The only other possible contaminants are K-dwarfs from the Halo/Spheroid. However, at a galactocentric distance of ~ 14 kpc, the space density of Halo/Spheroid K-dwarfs at $V \sim 22$ is ≈ 100 per square degree (*e.g.* Bahcall, Schmidt & Soneira 1983). With the caveat that *aposteriori* statistical estimates should only be a guide at best, the central part of the slit covers some 60 arcsec 2 , implying a probability of finding three or more Halo/Spheroid K-dwarfs in this part of the slit by chance, of a few parts in ten thousand. Factoring in the probability of the agreement in velocities, leads to a combined probability of less than one part in a million of this being a random contaminating Galactic sample. Since Antlia is also located well away from any other sources of possible near-Galactic contamination such as the Sagittarius Dwarf tidal stream, or the Magellanic Stream, we conclude that stars B, C and D are members of Antlia and that hence the optical helio-centric velocity of Antlia is 351 ± 15 km/s.

Our determination of the optical velocity for Antlia closely matches the HI velocity for this galaxy (Fouqué *et al.* and Skillman, private communication). Thus our results combined with those of Fouqué *et al.* unequivocally show that Antlia contains modest amounts, ($\approx 8 \times 10^5 M_\odot$), of HI gas centered on the optical position of the galaxy. This makes Antlia similar to LGS 3, another out-lying low surface brightness galaxy which

contains HI, and as with LGS 3, Antlia shows little evidence of recent star formation.

REFERENCES

Bahcall J.N., Schmidt M. & Soneira R.M. 1983, *ApJ*, 265, 730
Blitz L. & Robishaw T. 2000, *ApJ* in press, (astro-ph/0001142)
Braun R. & Burton W.B. 2000 *A&A*, 354, 853
Carignan C., Demers S., & Côte S., 1991 *ApJL*, 381, 13
Carignan C., Beaulieu S., Côte S., Demers S., Mateo M., 1998 *AJ*, 116, 1690
Da Costa G.S., Armandroff T.E. & Norris J.E. 1992, *AJ*, 104, 154
Fouqué R., Bottinelli L., Durand N., Gouguenheim L. & Patural 1990 *A&AS*, 86, 473
Hargreaves J.C., Gilmore G., Irwin M.J. & Carter D. 1994 *MNRAS*, 269, 957
Harris W.E. 1996 *AJ*, 112, 1487
Lavery R.J. & Mighell K.J. 1992 *AJ*, 103, 81
Oosterloo T., Da Costa G.S., Staveley-Smith L. 1996 *AJ*, 112, 1969
Osterbrock D.E., & Martel A. 1992 *PASP*, 104, 76
St-Germain J., Carignan C., Côte S., Oosterloo T. 1999 *AJ*, 118, 1235
Tolstoy E. 1999, review in the proceedings of the VLT Opening Symposium, Parallel Workshop 2: “Starway to the Universe”, March 1999, in press (astro-ph/9907029)
Tolstoy E., Gallagher J.S., Greggio L., Tosi M., De Marchi G., Romaniello M., Minniti D. & Zijlstra A.A. 2000, *ESO Messenger*, 99, 16
Whiting A.B., Irwin M.J. & Hau G.K.T. 1997 *AJ*, 114, 996
Whiting A.B., Hau G.K.T. & Irwin M.J. 1999 *AJ*, 118, 2767
Young L.M., & Lo K.Y. 1997 *AJ*, 490, 710

Table 1: The Galaxy Sample

Object	Distance (kpc)	M_V	type	ref
Antlia	1235	−10.8	dIrr/dSph	Whiting <i>et al.</i> 1997
Cetus	800	−10.1	dSph	Fouqué <i>et al.</i> 1990
Tucana	880	−9.6	dSph	Whiting <i>et al.</i> 1999
				Lavery & Mighell 1992

Table 2: The Observations

Date	Begin UT	Object	Exptime (secs)	Airmass	Seeing (arcsec)	Comments
11May99	23:53	Rup 106-1	150	1.2	1.3	Light Cirrus
12May99	00:12	HD 80170-1	1	1.1	0.85	
	00:29	Antlia-1	5400	1.1	0.7-1.4	Rapidly deteriorating seeing
	02:11	HD 92588	1	1.3	1.9	
6June99	00:04	Antlia-2	5400	1.2	0.7-1.6	Highly variable seeing
	01:51	Rup 106-2	150	1.2	1.5	
	02:13	HD 80170-2	1	2.4	0.95	
	02:25	HD 107328	1	1.4	0.9	
	02:48	Rup 106-3	150	1.3	1.1	
26July99	07:16	Pal 12	150	1.0	1.0	Cloudy, full Moon
	07:32	HD 203638	1	1.1	1.0	data too poor to use
24Aug99	05:14	HD 223647-1	1	1.9	1.25	Full Moon and thick cirrus
	05:40	NGC 6752-1	250	1.7	1.15	
	06:10	Tucana-1	5400	1.4	1.1-1.7	
	07:56	HD 223647-2	6	1.9	1.85	
	08:13	Tucana-2	5400	1.7	1.3-2.1	
	09:59	HD 223647-3	6	2.0	1.5	
26Aug99	03:49	NGC 6752-2	250	1.7	0.5	Full Moon
	04:09	HD 223647-4	1	1.9	0.5	
	04:11	HD 223647-5	1	1.9	0.5	
	04:36	Cetus-1	5400	1.1	0.5-0.8	Seeing deteriorating
	06:31	HD 693-1	1	1.0	0.7	
	06:34	HD 693-2	1	1.0	0.7	
	06:46	Cetus-2	5400	1.07	0.55-1.1	
	08:32	HD 8779-1	1	1.1	0.9	
	08:35	HD 8779-2	1	1.1	0.9	

Table 3: The Calibrators

Object	Class	V	v_{\odot} km/s	Ref
Rup 106	Cluster	10.9	–44.0	Da Costa <i>et al.</i> 1992
NGC 6752	Cluster	5.4	–27.9	Harris 1996
Pal 12	Cluster	11.99	+27.8	Harris 1996
HD 80170	K5 III-IV	5.33	+0.0	
HD 92588	K1 IV	6.26	+42.8	
HD 107328	K1 III	4.96	+35.7	
HD 223647	G5 III	5.11	+13.8	
HD 693 [†]	F6 V	4.89	+14.7	
HD 8779	K0 III	6.41	–5.0	

[†]Not used due to large template mismatch

Table 4: Individual Results

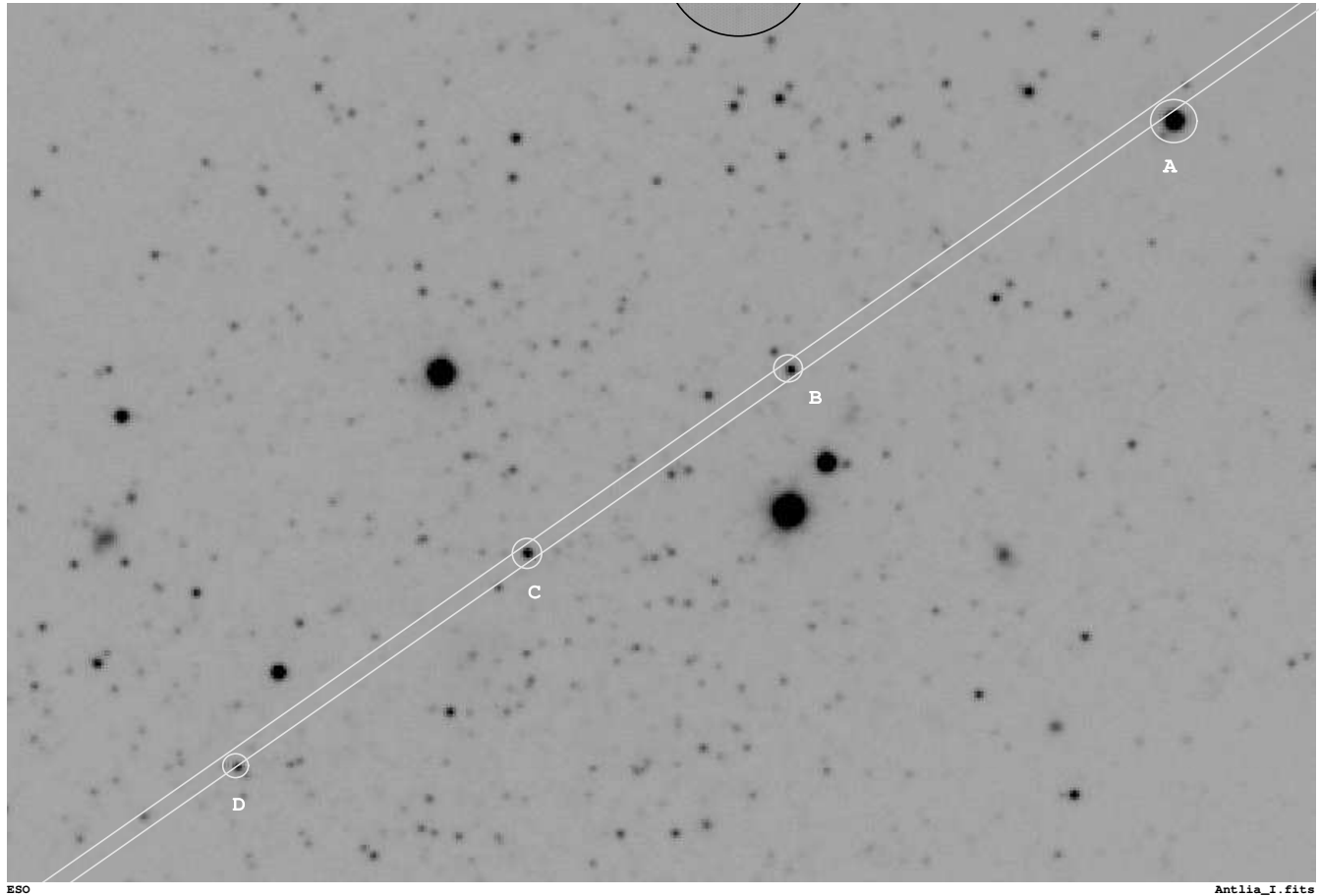
Object	v_{obs} (km/s)	Temp. Corr (km/s)	Helio Corr. (km/s)	Flex. Corr (km/s)	v_r (km/s)
HD 107328	+0.0	+63.3	-27.6	+0.0	+35.7
HD 80170-1	-30.1	+63.3	-17.2	-7.9	+8.1
HD 80170-2	+4.2	+63.3	-18.2	-35.5	+13.8
HD 92588	+1.3	+63.3	-26.9	-3.9	+33.8
HD 223647-1	+18.9	+63.3	-8.6	-55.3	+18.3
HD 223647-2	+19.9	+63.3	-8.6	-61.0	+13.6
HD 223647-3	+11.9	+63.3	-8.6	-59.2	+7.4
HD 223647-4	+11.9	+63.3	-8.6	-35.5	+31.1
HD 223647-5	-1.2	+63.3	-8.6	-23.7	+29.8
HD 8779-1	-58.3	+63.3	+21.2	-11.8	+14.4
HD 8779-2	-61.2	+63.3	+21.2	-7.9	+15.4
NGC 6752-1	-45.1	+63.3	-18.5	-19.0	-19.3
NGC 6752-2	-53.3	+63.3	-18.5	-11.9	-20.4
Rup 106-1-a	+250.5	+63.3	-6.8	-19.7	+287.3
Rup 106-1-b	+5.7	+63.3	-6.8	-19.7	+42.5
Rup 106-1-c	-11.4	+63.3	-6.8	-19.7	+25.4
Rup 106-1-d	-50.9	+63.3	-6.8	-19.7	-14.1
Rup 106-1-e	-87.1	+63.3	-6.8	-19.7	-50.4
Rup 106-1-unresolved	-50:	+63.3	-6.8	-19.7	-14:
Rup 106-2-a	+188.9	+63.3	-14.2	+7.9	+245.9
Rup 106-2-b	-34.4	+63.3	-14.2	+7.9	+22.6
Rup 106-2-c	-28.0	+63.3	-14.2	+7.9	+29.0
Rup 106-2-d	-53.1	+63.3	-14.2	+7.9	+3.9
Rup 106-2-e	-57.7	+63.3	-14.2	+7.9	-0.7
Rup 106-3-w	+27.3	+63.3	-14.2	-11.8	+64.6
Rup 106-3-x	-10.9	+63.3	-14.2	-11.8	+26.4
Rup 106-3-y	-18.9	+63.3	-14.2	-11.8	+18.4
Rup 106-3-z	-84.1	+63.3	-14.2	-11.8	-46.8
Antlia-1-a	-41.8	+63.3	-21.6	+4.7	-4.6
Antlia-1-b	+353.2	+63.3	-21.6	+4.7	+399.6
Antlia-1-c	+308.1	+63.3	-21.6	+4.7	+354.5
Antlia-1-d	+300:	+63.3	-21.6	+4.7	+346:
Antlia-1-e	-142:	+63.3	-21.6	+4.7	-96:
Antlia-1-unresolved	+380:	+63.3	-21.6	+4.7	+426:
Antlia-2-b	+329.1	+63.3	-23.6	+0.5	+371.1
Antlia-2-c	+303.8	+63.3	-23.6	+0.5	+344.0
Antlia-2-d	+318.1	+63.3	-23.6	+0.5	+358.3
Antlia-2-e	-183.6	+63.3	-23.6	+0.5	-143.4
Antlia-2-unresolved	+366.9	+63.3	-23.6	+0.5	+407.1

Table 5: Summary of Results

Object	$\langle v_r \text{ obs} \rangle$ (km/s)	$v_r \text{ known}$ (km/s)	Comments
HD 107328	$+35.7 \pm 0.0^*$	$+35.7 \pm 0.3$	RV template
HD 80170	$+10.9 \pm 7.8$	$+0.0 \pm 0.2$	RV standard
HD 92588	$+33.8 \pm 6.9$	$+42.8 \pm 0.1$	RV standard
HD 223647	$+20.0 \pm 7.4$	$+13.8 \pm 0.4$	RV standard
HD 8779	$+14.9 \pm 8.3$	-5.0 ± 0.6	RV standard
Rup 106	$:^{\dagger}$	-44.0 ± 3.0	Cluster Standard
NGC 6752	-19.8 ± 6.7	-27.9 ± 0.8	Cluster Standard
Antlia-1-bcd	363.1 ± 16.4	361 ± 2	HI velocity from Fouqué <i>et al.</i>
Antlia-2-bcd	335.3 ± 17.1		
Antlia-1,2-bcd	349.5 ± 11.7		HD 107328 as template
Antlia-1,2-bcd	351.4 ± 12.9		NGC6752 as template

*This is the rv primary standard, and so by definition has a relative rv of 0.0 with no error.

†Not useable, due to poor s/n, and a very crowded field of view



Feb 16, 2000 at 17:34:50

Fig. 1.— The central 4 arcmin of the Antlia galaxy with the adopted slit position marked. North is up and East is left. This plot comes from the FIMS, observation preparation tool output. The image is a combined 5400sec of I filter observations made with FORS1 for FORS1 Science Verification in January 1999. Marked on the image are 4 of the 5 stars identified in our slit and for which individual spectra could be usefully extracted.

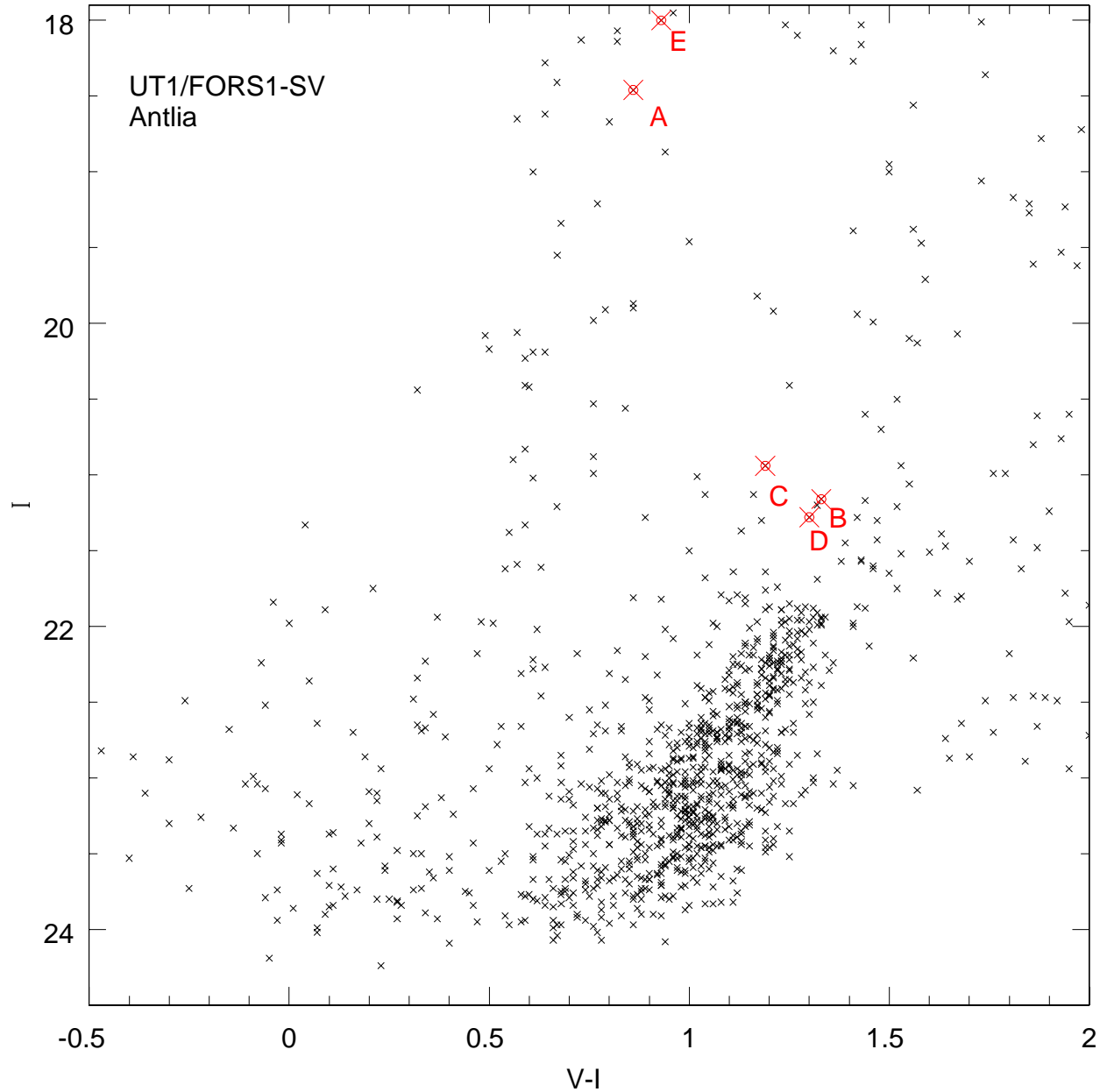


Fig. 2.— An Antlia (I, V-I) Colour-Magnitude Diagram made from FORS1 Science Verification data taken in January 1999. Plotted in large cross symbols are stars in the slit for which we could extract individual spectra. The labels correspond to the letters in Figure 1 and in Table 4. Objects B, C, D lie near the tip of the red giant branch and have similar velocities (see Table 4).

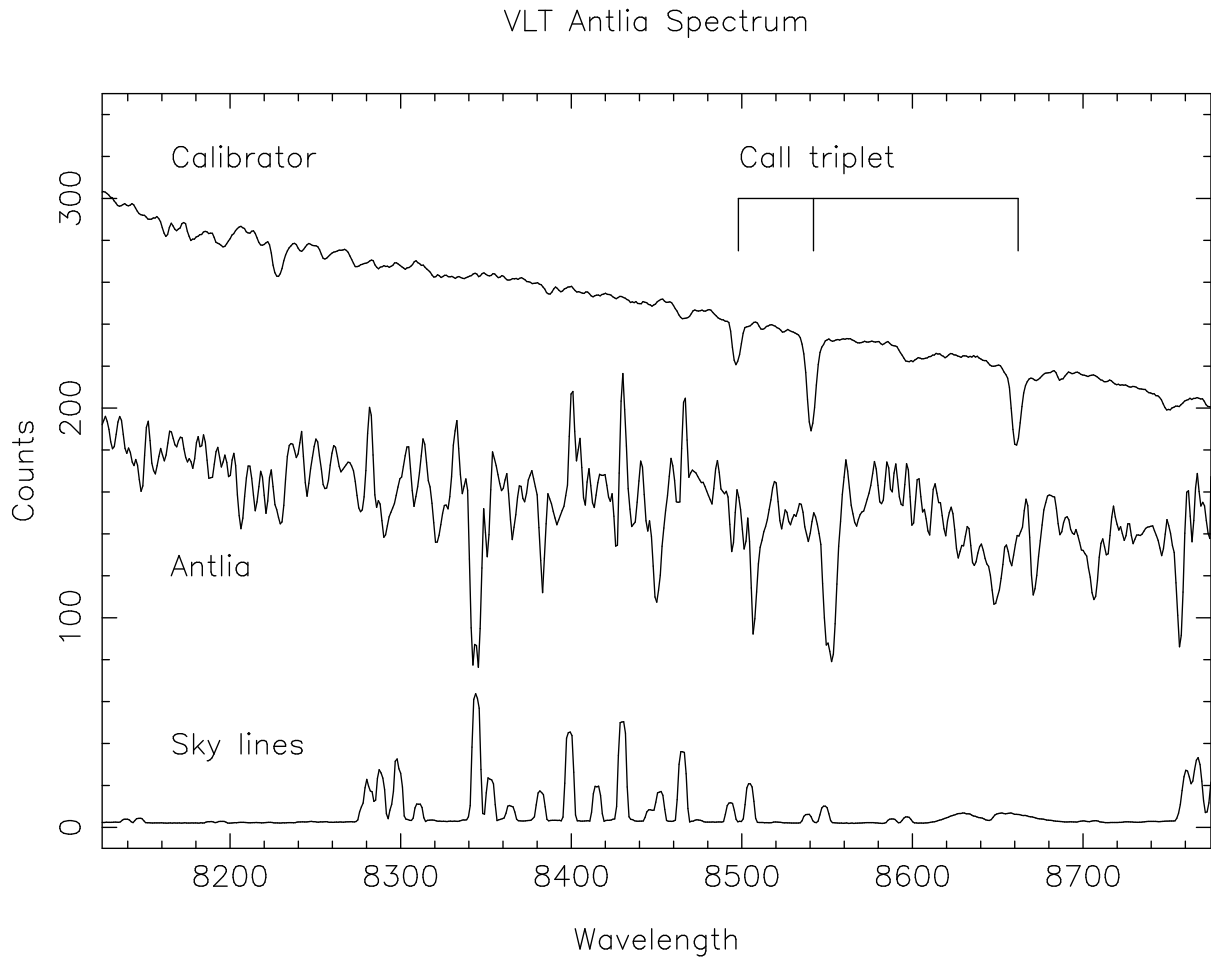


Fig. 3.— Here we plot the combined Antlia spectrum of objects b, c and d from both observation epochs. Also plotted for comparison above Antlia is the spectrum of the globular cluster spectrum of NGC 6752 (Calibrator). The Ca II triplet lines for Antlia are clearly redshifted by $\approx 10\text{\AA}$ with respect to the calibrator cluster. Also included at the bottom of the plot is a scaled down (by a factor of 75) sky spectrum illustrating the problems of residual sky line contamination.

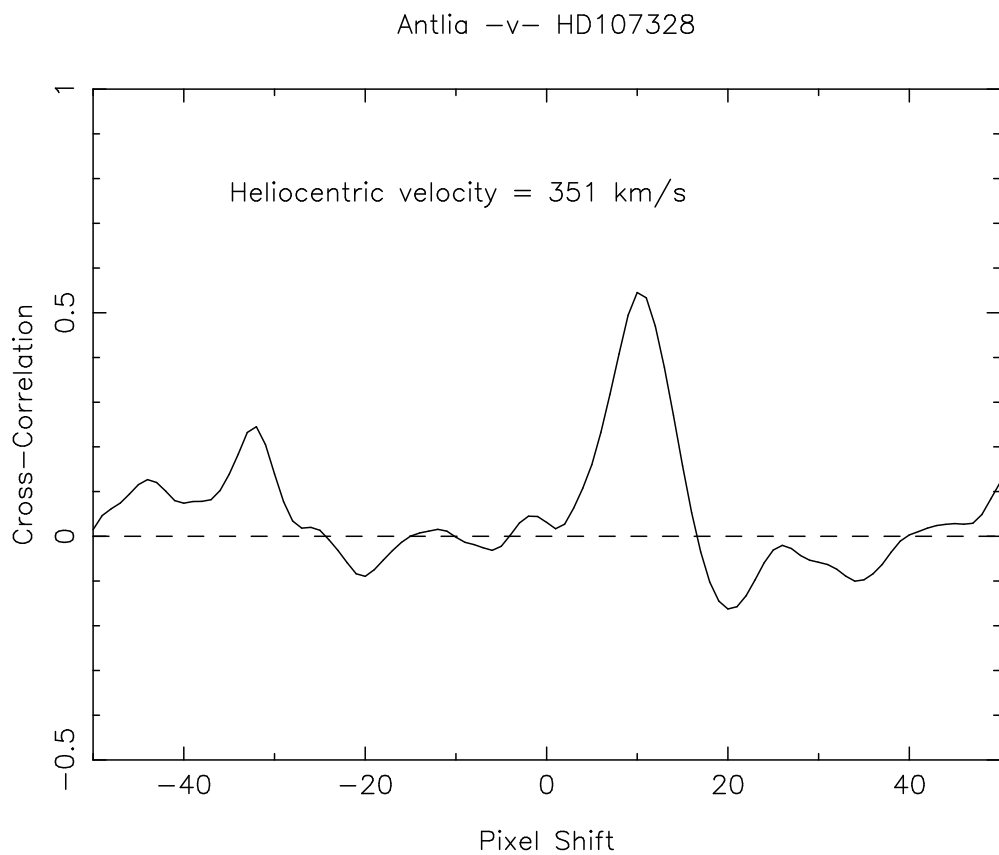


Fig. 4.— The cross-correlation of the Antlia spectrum, shown in Figure 3, against the HD 107328 template spectrum. No template, flexure or helio-centric corrections have been made for this plot.